J Nanopart Res (2011) 13:5485–5495
DOI 10.1007/s11051-011-0536-3

RESEARCH PAPER

Protein-assisted synthesis route of metal nanoparticles: exploration of key chemistry of the biomolecule

Nirmal Goswami · Ranajay Saha · Samir Kumar Pal

Received: 16 March 2011 / Accepted: 29 July 2011 / Published online: 13 August 2011

Abstract Essentially, biomolecule assisted synthesis of inorganic nanoparticles can be divided into two categories. One uses multi-domain protein cages (template) and other relies on the self-assembly of the biomolecules including small peptides, DNA, and denatured protein. Protein templated synthesis of various nanomaterials is relatively well understood as the cages of the biological macromolecules and their specific interaction with inorganic ions ultimately dictate the size and crystallinity of the nanomaterials. On the other hand formation of nanoparticles using protein in the cost of the native structural integrity for the self-assembly is not well understood till date. In the present work we report a protein-assisted synthesis route to prepare highly crystalline 3–5 nm gold nanoparticles, which relies systematic thermal denaturation of a number of proteins and protein mixture from *Escherichia coli* in absence of any reducing agent. By using UV–vis, circular dichroism spectroscopy, and high-resolution transmission electron microscopy we have explored details of the associated biochemistry of the proteins dictating kinetics, size, and crystallinity of the nanoparticles. The kinetics of nanoparticles formation in this route, which is sigmoidal in nature, has been modelled in a simple scheme of autocatalytic process. Interestingly, the protein-capped as prepared Au nanoparticles are found to serve as effective catalyst to activate the reduction of 4-nitrophenol in the presence of $NaBH_4$. The kinetic data obtained by monitoring the reduction of 4-nitrophenol by UV/vis-spectroscopy revealing the efficient catalytic activity of the nanoparticles have been explained in terms of the Langmuir–Hinshelwood model. The methodology and the details of the protein chemistry presented here may find relevance in the protein-assisted synthesis of inorganic nanostructures in general.

Keywords Protein-capped gold nanoparticle · High-resolution transmission electron microscopy · Reduction of 4-nitrophenylacetate · Autocatalysis of gold nanoparticle · Langmuir–Hinshelwood surface catalysis · Synthesis mechanism

N. Goswami · R. Saha · S. K. Pal (✉)
Department of Chemical, Biological & Macromolecular Sciences, Unit for Nano Science & Technology, S. N. Bose National Centre for Basic Sciences, Block JD, Sector III, Salt Lake, Kolkata 700098, India
e-mail: skpal@bose.res.in

Present Address:
S. K. Pal
Arthur Amos Noyes Laboratory of Chemical Physics, California Institute of Technology (CALTECH), 1200 East California Boulevard, Pasadena, CA 91125, USA

Introduction

Inorganic nanoparticles of controlled size have been of great interest recently for a number of possible applications in electronic or optical materials, as well as in catalysis (Jin 2001; Sun and Xia 2002; Narayanan

and El-Sayed 2004; Ghosh and Pal 2007; Tian et al. 2007; Vajda et al. 2009). For example, Au nanoparticles have attracted much attention in chemistry and material science because of their good biocompatibility, facile synthesis (Burda et al. 2005), and conjugation to a variety of bimolecular ligands, antibodies, and other targeting moieties (Katz and Willner 2004), which make them suitable for the use in biochemical sensing and detection (Storhoff et al. 1998; Riboh et al. 2003; Shafer-Peltier et al. 2003). Biocompatibility of the inorganic nanoparticles often relies on two synthetic strategies; one uses nano-cages of biological macromolecules [e.g., ferritin (Kramer et al. 2004; Flenniken et al. 2009), apoferritin (Kim et al. 2009), heat-shock protein (Klem et al. 2005), etc.] and the other method is involved with the self assembling property of the biological macromolecules [e.g., protein (Xie et al. 2009), peptides (Dinda et al. 2010), DNA (Mirkin et al. 1996; Loweth et al. 1999), etc.]. The first synthetic strategy is quite straightforward as the size and its interaction with the nano-cages dictate the quality of the synthesized nanoparticles (Flenniken et al. 2009; Kim et al. 2009). On the other hand the second route essentially depends on the primary condition for the nucleation and capping by the biomolecules, which is relatively less explored. One of the recent studies uses small peptides to prepare the nanoparticles (Tan et al. 2010). It has been demonstrated that the reduction capability and the net charge of a peptide play the key role on the nucleation and growth of the Au nanoparticles. However, a detailed study highlighting every step involved in the formation of nanoparticles using large protein molecules is absent in the literature and is the motive of this study.

Herein, we report the facile preparation of "green" Au nanoparticles (NPs) in a number of protein solutions starting from globular proteins to enzyme and finally protein mixture extract from *Escherichia coli*, a gram negative bacterium, without the addition of any reducing agent. The nucleation of NPs in the protein environments, which is the consequence of electron transfer from protein to the metal ions, is observed to be dependent on the melting temperature of the host protein. However, time required to start the nucleation (induction time) is also found to be protein-specific. Here, we have attempted to rationalize the protein-assisted formation of NPs in a simple analytical model of autocatalysis. This model is evolving under the impudence of two distinct reactions. The first of these is the thermal denaturation of the protein structure under thermal condition and the second one is reversible autocatalytic process in which Au NP is the autocatalytic species (both the product and catalyst for the reaction). The obtained nanoparticles are characterized by UV–vis absorption spectroscopy, high-resolution transmission electron microscopy (HRTEM). The change in the protein structure at various temperatures has been followed by circular dichroism (CD) spectroscopy. In this work we have also demonstrated that the protein-capped NPs can be utilized as an efficient catalyst for the degradation of 4-nitrophenylacetate (4-NPA) using $NaBH_4$ as the hydrogen donor. The reduction of 4-NPA to 4-aminophenol (4-AP) has industrial importance as 4-AP is a commercially important intermediate for the manufacture of analgesic and antipyretic drugs. Although a number of researchers have extensively studied the catalytic reduction of 4-nitrophenol (4-NP) by $NaBH_4$ using polymer/resin bead-supported metal NPs (Esumi et al. 2004; Praharaj et al. 2004; Zhang et al. 2009; Saha et al. 2010) the synthesis of protein-capped Au NPs and the use of these NPs without any support for this catalytic purpose has not been attempted earlier. The kinetics of the catalysis is observed to follow Langmuir–Hinshelwood model of surface mediated catalysis reaction.

Materials and methods

All the proteins and chemicals [human serum albumin (HSA), bovine serum albumin (BSA), subtilisin Carlsberg (SC), chymotrypsin (CHT), Tris–Cl, $NaBH_4$, 4-NPA, $HAuCl_4$, and phosphate buffer] were obtained from Sigma. Double distilled water was used for preparation of aqueous solutions. Steady-state absorption was measured with a Shimadzu UV-2450 spectrophotometer. The CD spectrum was measured in a Jasco 815 spectropolarimeter with a Peltier setup for the temperature-dependent measurements. CD studies were done with 10 mm path length cell. Thermal unfolding of HSA was monitored by recording far-UV CD at 222 nm as a function of temperature. The temperature was raised from 20 to 90 °C in 2 °C step with 2 min equilibration time at each temperature. The unfolding curves were constructed after converting the CD values to fraction unfolded (Kamal and Behere 2002). A JEOL JEM-2100 HRTEM equipped with an energy dispersive X-ray (EDAX) spectrometer was

used to characterize the particle size and individual shape of the nanoparticles and to analyze their elemental composition. TEM samples were prepared by dropping sample stock solutions onto a 300 mesh carbon coated copper grid and dried overnight in air.

Synthesis of Au@protein nanobioconjugates

The Au@protein nanobioconjugates were prepared by the following procedure: 3 mL, 20 μM protein solutions were prepared in 20 mM phosphate buffer solution. Then 60 μL 100 mM $HAuCl_4$ solution was added so that protein:$HAuCl_4$ ratio was maintained at 1:100. A detailed temperature-dependent study was performed starting from 30 °C for each mixture and it has been found that when the mixtures were heated at 76, 75, and 60 °C for HSA, BSA, and SC, respectively, the colours of the solutions were changed from light yellow to reddish brown. Such colour transition is indicative of changes in the metal oxidation state. In this case, Au(III) is reduced to Au(0) by protein in the phosphate buffer solution. We have not observed any sign of NP formation at room temperature for several days.

Extraction of protein mixture from *Escherichia coli*

Single colony of *E. coli* was inoculated in 100 mL Luria Broth (LB) and then incubated overnight at 37 °C with shaking. The obtained cells from 100 mL culture were harvested by centrifugation (6,000 rpm) for 5 min, washed twice with 0.1 M Tris–Cl (pH 8.2) and recentrifuged. The cells were then suspended in 2 mL lysis buffer and incubated for 20 min. Next it was allowed to freeze thaw for three times giving 1 min incubation at ice. Finally the cell suspension was sonicated (80 amplitude and 0.6 cps) for 10 min and the supernatant collected by centrifugation (10,000 rpm) for 15 min at 4 °C was the protein.

Synthesis of Au@*Escherichia coli* protein extracts nanobioconjugates

The Au@*E. coli* extract protein conjugates were prepared by the following method: 1 mL protein extract solution was diluted with 1 mL lysis buffer and then 60 μL 100 mM $HAuCl_4$ solution was added. The whole mixture was heated at 70 °C so that all the proteins present in the mixture were denatured. After 10 min the colours of the solutions were changed from light yellow to deep brown indicating the formation of Au NPs.

Analytical modelling

Kinetics of nanoparticle formation

In the case of the autocatalytic reactions, the modified protein–salt conjugate serves as a substrate in reactions. The general mechanism of the nanoparticle formation can be written as shown in the following equations:

$$\text{Nucleation} : \text{EL} \xrightarrow{k_1} \text{FP (slow)} \tag{1}$$

$$\text{Growth} : \text{EL} + \text{FP} \xrightarrow{k_2} 2\text{FP (fast)} \tag{2}$$

where, L represents the salt i.e., $AuCl_4^-$, and E and F represent two different forms of protein where F-form is more perturbed than E-form, and k_1 and k_2 are the rate constants of the slow and fast step, respectively. Here, EL denotes the protein–salt conjugate and FP denotes the protein–nanoparticle conjugate. The corresponding rate equation (assuming first-order reaction) of the first step can be written as,

$$[\text{FP}] = [\text{EL}]_0(1 - \exp^{-k_1 t}) \tag{3}$$

where $[\text{EL}]_0$ and [FP] are the concentration of the E-form of the protein–salt conjugate at the initial time and the concentration of the protein–nanoparticle conjugate at time $= t$, respectively.

Equation (2) is the autocatalytic step (Drummond et al. 2010). For this autocatalytic reaction the concentration of the product can be written as,

$$[\text{FP}] = \frac{[\text{EL}]_0 + [\text{FP}]_0}{1 + \frac{[\text{EL}]_0}{[\text{FP}]_0}\exp^{-\left([\text{EL}]_0 + [\text{FP}]_0\right)k_2 t}} \tag{4}$$

So, the total concentration of the protein-capped nanoparticles is obtained by the linear combination of Eqs. (3 and 4) and thus it can be written as:

$$[\text{FP}] = m \times \left(\frac{[\text{EL}]_0 + [\text{FP}]_0}{1 + \frac{[\text{EL}]_0}{[\text{FP}]_0}\exp^{-\left([\text{EL}]_0 + [\text{FP}]_0\right)k_2 t}}\right) + n \times \left([\text{EL}]_0 \times \left(1 - \exp^{k_1 t}\right)\right) \tag{5}$$

where m and n denote the contributions of the fast and slow step, respectively.

Catalysis of 4-nitrophenyl acetate (4-NPA) reduction by the nanoparticles

The catalytic reduction of 4-NPA by sodium borohydride on the surface of the Au NPs is presented as,

$$\begin{aligned} &CH_3CO_2C_6H_4NO_2(\text{4-NPA}) \\ &\quad + NaBH_4 \xrightarrow{\text{AuNP}} C_6H_7NO(\text{4-AP}) \end{aligned} \tag{6}$$

In this study, the obtained kinetic data of 4-NPA reduction are fitted in a first-order rate equation as an excess of borohydride is used compared to 4-NPA. The apparent rate constant (k_{app}) is assumed to be proportional to the surface area (S) of the metal nanoparticles present in the system (Mei et al. 2005, 2007; Panigrahi et al. 2007). Hence,

$$r = -\frac{dc_{NP}}{dt} = k_{app}c_{NP} = k_S S c_{NP} \tag{7}$$

where r is the rate of the reaction, c_{NP} is the concentration of 4-NP, and k_S is the rate constant of the reaction. Herein, we focus on a complete analysis of the heterogeneous reduction of 4-NPA in the presence of Au NPs. We have demonstrated (see later in the text) that the reaction is surface controlled and can be analyzed in terms of the Langmuir–Hinshelwood mechanism (Belohlav and Zamostny 2000; Xu et al. 2008, 2009). In this mechanism it is assumed that both reactants need to be adsorbed on the surface of the catalyst. The overall rate-determining step is governed by the rate of surface adsorption of the reactants. In addition to the analysis of the reaction rate, the dependence of the k_{app} on the various parameters will be analyzed quantitatively and derived from the Langmuir–Hinshelwood analysis.

In this mechanism the adsorption of the reactants is modelled in terms of the Langmuir–Freundlich (LF) isotherm (Umpleby et al. 2001):

$$\theta_i = \frac{(k_i c_i)^{n_i}}{1 + \sum_{j=1}^{N} (k_j c_j)^{n_j}} \tag{8}$$

Here, θ_i is the surface coverage of compound i, k_i is the adsorption constant of the respective component, and c_i is the concentration in solution. The exponent n is related to the heterogeneity of the sorbent. For a homogeneous material, n is equal to 1 whereas, when n is between 0 and 1 the material is heterogeneous. For homogeneous material ($n = 1$), the LF isotherm reduces to the Langmuir isotherm. Hence Eq. (7) can be written as,

$$r = k_S S \theta_{BH_4^-}^m \theta_{NP}^n = k_{app} c_{NP} \tag{9}$$

So, from Eq. (9) we get,

$$k_{app} = \frac{k_S S \left(k_{BH_4^-} c_{BH_4^-}\right)^m k_{NP}^n c_{NP}^{n-1}}{\left[1 + \left(k_{BH_4^-} c_{BH_4^-}\right)^m + \left(k_{NP} c_{NP}\right)^n\right]^2} \tag{10}$$

Here k_S is the molar rate constant per square meter of the catalyst and k_{NP} is the adsorption constant of nitrophenolate ion and k_{BH_4} is the adsorption constant of borohydride.

Results and discussion

Figure 1a shows the TEM image of Au@HSA nanobioconjugates. The image reveals that the nanobioconjugates are almost spherical in shape and follow a uniform narrow size distribution. Particle sizes have been estimated by fitting our experimental TEM data to be 3.1 nm [inset in Fig. 1a (right)]. The corresponding HRTEM image of the particles is shown in Fig. 1b. The interplanar distance of the fringes is measured to be about 0.24 nm, consistent with the distance between the (111) planes of the gold crystal lattice. The image in the inset of Fig. 1b represents the corresponding selected area electron diffraction (SAED) pattern which confirms the crystallinity of those particles. It has to be noted that the average size of 3.1 nm Au NPs obtained in the HSA@Au NPs solution, is also confirmed from TEM and absorption studies (see later in the text). Thus in our experimental conditions, the possibility of formation of free larger Au NPs of micrometre size (due to uncontrolled growth) is negligibly small as they are not revealed in the TEM images of the sample. A typical energy dispersive X-ray (EDAX) spectrum of Au@HSA sample is shown in the inset of Fig. 1a (left) revealing the presence of Au NPs. Figure 1c shows the HRTEM image of Au@BSA nanobioconjugates and the size distribution is shown as an inset of Fig. 1c.

It is well-known that the Au NPs of less than 10 nm exhibit a surface plasmon (SP) band in the visible region (~530 nm) (El-Brolossy et al. 2008). A change in absorbance or wavelength of the SP band (Link and El-Sayed 2000; Ung et al. 2001; Luo et al. 2004) provides a measure of particle size, shape, concentration, and dielectric medium properties.

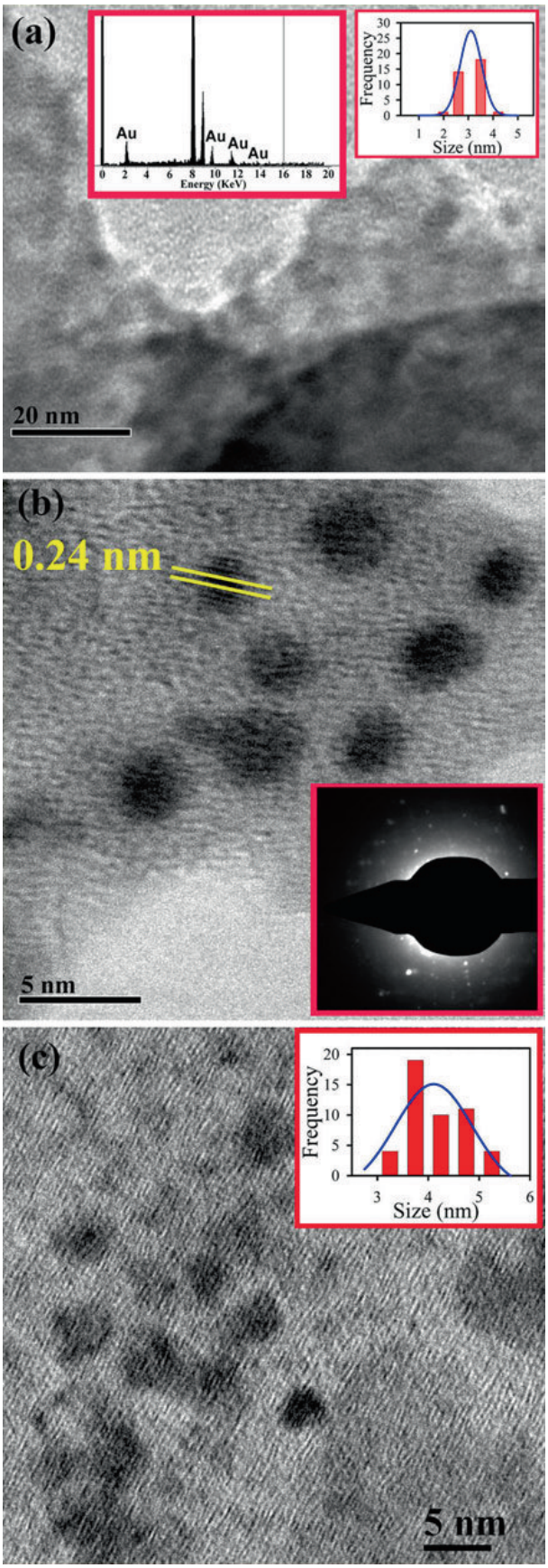

◀ **Fig. 1** **a** HRTEM of Au@HSA nanobioconjugates. The EDAX pattern (*left*) and the size distribution (*right*) of the sample are shown in the *insets*. **b** HRTEM image and SAED showing the crystalline structure of Au@HSA NPs. **c** HRTEM of Au@BSA nanobioconjugates. The size distribution of the sample is shown in the *inset*

Figure 2a shows the UV–vis spectra of the Au NPs conjugated with HSA, BSA, SC, and *E. coli* extract protein revealing SP bands at 530, 531, 540, and 600 nm, respectively. On the basis of Mie theory (Mie 1908) and its expanded versions (Doyle 1958; Zeman and Schatz 1987), information concerning nanoparticle sizes can be derived from the analysis of this absorption band. The average radius of Au NPs (spherical as revealed from HRTEM), can be approximately estimated from the resonance optical absorption spectrum as per the Mie scattering formula (Mie 1908)

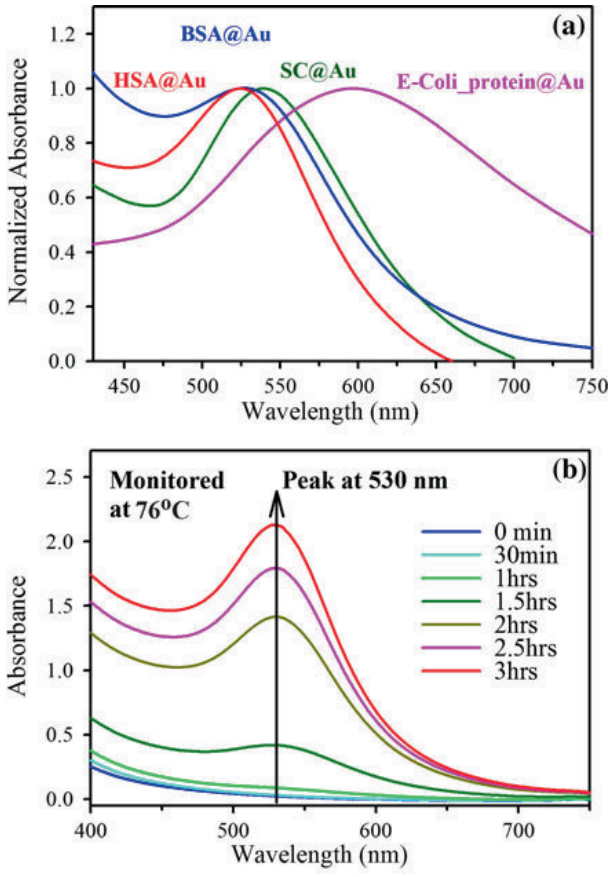

Fig. 2 **a** UV–vis spectra of Au NPs conjugated with various proteins, HSA, BSA, SC, and *E. coli* extract, respectively. **b** Time-resolved UV–vis spectra for one of the representative proteins (HSA) at 76 °C

$$r_{\text{metal}} = \frac{\upsilon_F}{\Delta\omega_{1/2}} = \frac{\upsilon_F}{2\pi c_0\left(\frac{\Delta\lambda}{\lambda_P^2}\right)} \tag{11}$$

where υ_F = Fermi velocity (1.39×10^6 m/s for Au) (Dhawan and Muth 2006) and $\Delta\omega_{1/2}$ is the full width at half-maximum (FWHM) of the surface plasmon resonance (SPR) absorption when plotted as a function of angular frequency ω, c_0 is the speed of light in vacuum, λ_P is the wavelength where absorption peak appears, and $\Delta\lambda$ gives the FWHM of the band. The average diameters of the NPs calculated using Eq. (11) is found to be in the range of 3.4, 3.5, and 3.7 nm for HSA, BSA, and SC, respectively, consistent with those observed in TEM studies. Relatively broad SP band of Au@*E. coli* extract indicates the broad size distribution which is mainly due to the mixture of proteins present in the solution. Figure 2b shows the UV–vis absorption spectra obtained at different time intervals after mixing with aqueous $AuCl_4^-$ solution with HSA in phosphate buffer at 76 °C temperature. Formation of Au nanoparticles in the colloidal solution was monitored from their absorption spectra as the small noble metal particles reveal absorption band in the UV–vis spectral region due to SPR (Bohren and Huffman 1983). The sharp absorption band peaking at 530 nm indicates a relatively high monodispersity, both in size and shape of the Au particles (Malikova et al. 2002), consistent with the HRTEM images. Long time stability of the Au NP in aqueous solutions (for several months) indicates that the HSA serves as capping agent. In the case of the other proteins, a similar trend was observed as that of the HSA.

The evolution of the optical density at 530 and 540 nm are presented for Au@HSA at 76 °C and Au@SC at 60 °C in Fig. 3a and b, respectively. It is apparent that for Au@HSA the optical density increases very slowly up to 120 min for HSA, indicating an induction time (t_0), then sharply increases and finally saturates at a constant value which corresponds to a complete reduction stage. The induction time became shorter when the concentration

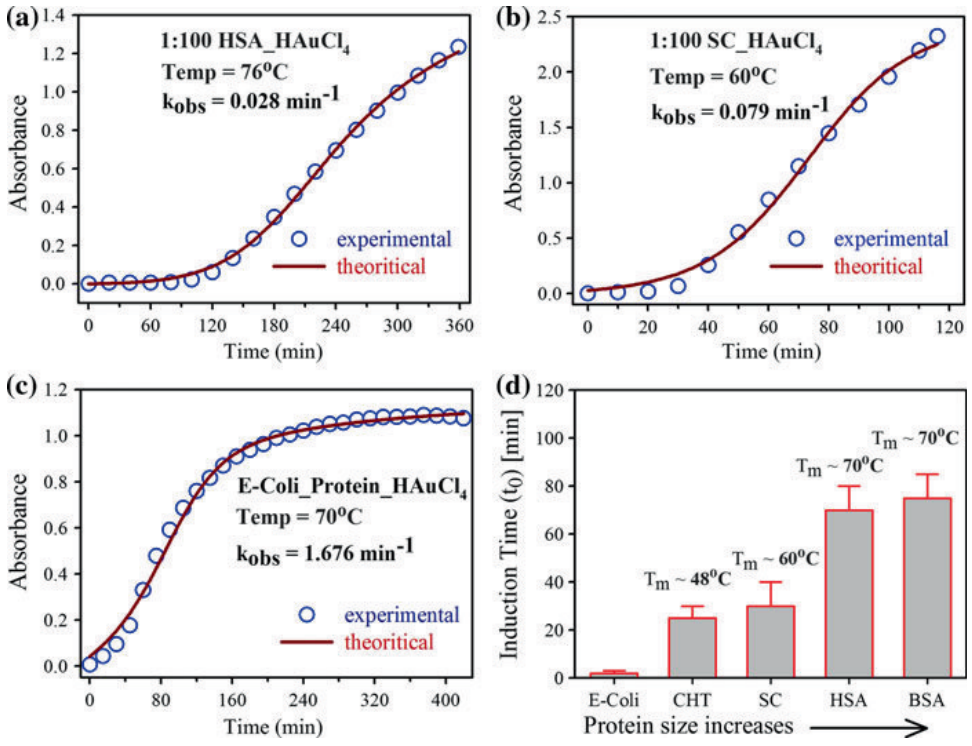

Fig. 3 **a** Time course of absorbance at 530 nm during the formation of Au NPs particles by HSA protein in phosphate buffer solution. **b** Similar curve at 540 nm by using SC in phosphate buffer solution. The *solid lines* are the theoretical curves generated by using Eq. (5). *Circles* are the experimental data for HSA and SC, respectively. **c** Absorbance kinetics of the Au NPs formation at 580 nm using *E. coli* extract as reducing agent. **d** Plot of induction time for different proteins. In all the cases (except *E. coli*) the protein–salt ratio has maintained to 1:100 where the protein concentration is fixed at 20 μM

of protein is increased. The most interesting information is the variation in induction period (shown in Fig. 3d) for protein to protein with same concentration. We assume that the size as well as the melting temperature is the predominant factor for the induction period. The denaturation of protein plays an important role in activating the reaction. From Fig. 3d, it is clear that proteins having low melting temperature have small induction time and vice versa. Second, based on the experimental results, we have proposed an analytical model for the kinetics of the Au@protein system (Eqs. 1 and 2) which suggests that autocatalysis is involved for the synthesis process. This model suggests that during the induction period, nucleations of the NPs are slowly formed and can be considered as seeds. The formation of these nucleations, or seeds, catalyzes the reduction processes and thus in the next stage (Eq. 2), seed-mediated nucleation and growth occur simultaneously, and the number of particles rapidly increases as the reaction progresses. Here, the strong capping property of the proteins inhibits the nanoparticle growth, thus generating high monodispersity. The solid lines in Fig. 3 refer to the fit of the experimental data with Eq. (5) while Table 1 shows the fitting parameters. This model gives a quantitative explanation of the kinetic data shown in Fig. 3 for all the proteins. In particular, it explains the dependence of induction time on k_1 i.e., higher the value of rate constant (k_1), smaller the induction time and vice versa. The autocatalytic rate constant (k_2) as revealed from Table 1, demonstrates that larger proteins (i.e., HSA or BSA) are less active than smaller proteins (i.e., SC, CHT or *E. coli* extract) for the growth of NPs. The overwhelming contribution of growth step compared to that of the nucleation is clear from Table 1. In simple autocatalytic reaction (Huang et al. 1993) the overall rate is obtained by plotting ln $[a/(1-a)]$ versus time (data not shown) where $a = [\mathrm{OD}(t)/\mathrm{OD}(\infty)]$ and $\mathrm{OD}(t)$ and $\mathrm{OD}(\infty)$ are the optical densities at times t and ∞, respectively. The rate constant (k_{obs}) is obtained from the slopes of these plots. In case of Au@HSA the value of k_{obs} is found to be 0.028/min.

Table 1 List of the parameters obtained from the analytical model of particle formation

Protein	k_1 (min^{-1})	k_2 ($\mathrm{M}^{-1}\ \mathrm{min}^{-1}$)	m (%)	n (%)
HSA	1.245×10^{-4}	0.015	0.91 (91)	0.09 (9)
SC	4.677×10^{-4}	0.020	0.79 (79)	0.21 (21)
E. coli extract	3.178×10^{-1}	3.488	0.72 (72)	0.28 (28)

It is well-known that conformational changes occur when proteins adsorb onto nanoparticles (Fei and Perretts 2009). It has been demonstrated that in the presence of gold nanoparticles, BSA shows a decrease in α-helical structure, as detected by CD, and a significant increase in sheet and turn structures, as detected by Fourier transform infrared (FTIR) spectroscopy (Shang et al. 2007). In our study, although proteins are denatured at the particle formation temperature yet more conformational changes occur with time due to the intrinsic properties of the protein combined with features of the nanoparticles, such as surface chemistry and surface curvature. Figure 4 shows the decrease of molar ellipticity with time which describes more structural perturbation. The rate constant of protein conformational change (k_{den}) is obtained by fitting the experimental data with first-order exponential equation. It has been found that in case of Au@HSA system the value of k_{den} (0.029/min) is very much comparable to the value of k_{obs} (0.028/min) which reveals more conformational change during the autocatalytic process. Figure 3c represents the evolution of the SPR peak at 580 nm with time for a mixture of proteins obtained from *E. coli* extract. Here, the shorter induction time is probably due to the mixture of protein present in the extract. At higher temperature relatively smaller proteins are denatured very quickly resulting very fast reduction of Au ions. The role of DNA in the *E. coli* extract in the formation of Au NPs has been ruled out as a control study on DNA–Au(III) ion mixture at 75 °C fails to reveal any Au NPs even after 2 h. Generalized two-step mechanism for autocatalytic growth is shown in Scheme 1 where the first step is the slow nucleation step and the second step indicates the seed-mediated autocatalytic growth.

In this study, the catalytic function of Au@protein nanobioconjugates is substantiated by carrying out the reduction of aqueous 4-NPA, which has a peak at 276 nm in the UV–vis. spectrum (Fig. 5a, curve I). Addition of sodium borohydride to 4-NPA immediately results in a shift in the peak to 400 nm with intensification of yellow colour of the solution (Fig. 5a, curve II) due to nitrophenolate ion

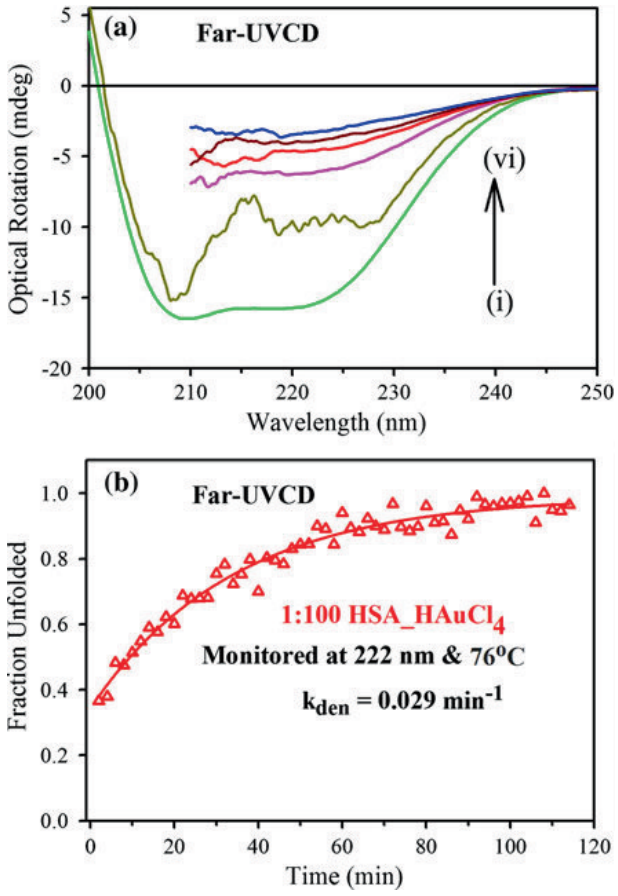

Fig. 4 **a** Far-UV CD spectra of (*i*) 1 μM HSA and 1:100 HSA–$HAuCl_4$ at (*ii*) initially at room temperature (*iii*) after 30 min, (*iv*) after 60 min, (*v*) after 90 min, (*vi*) after 180 min. (*iii–vi*) At 76 °C temperature. **b** Far-UV CD spectrum of 1:100 HSA–$HAuCl_4$ system monitored at 222 nm and 76 °C temperature

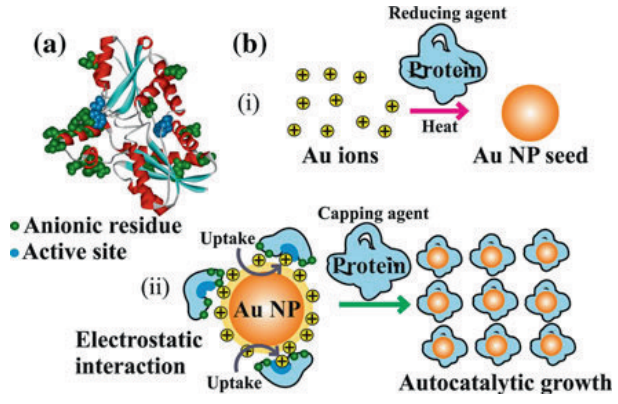

Scheme 1 **a** Molecular structure of subtilisin Carlsberg. **b** Generalized two-step [(i) and (ii)] mechanism for solution-phase Au nanoparticle synthesis

formation. In the absence of any catalyst, the peak at 400 nm remains unaltered even for 2 days. Addition of Au@protein nanobioconjugates to the yellow colour of the nitrophenolate ion solution immediately results the diminution of 400 nm peak with intensification of a new peak at ~297 nm (Fig. 5a, curve III) because of the reduction of 4-nitrophenolate species to 4-AP. A control experiment with denatured proteins devoid of gold nanoparticles did not provide any signature of 4-AP under the same experimental condition. The generation of 4-AP confirms the catalytic activity of the Au nanoparticles for the reduction of 4-nitrophenolate in aqueous solution. Figure 5, b shows that after the addition of Au nanoparticles the absorption peak at 400 nm gradually drops with time. Figure 5c shows the time dependence results obtained from the reaction conducted at room temperature. This observation indicates that upon the addition of Au@protein nanobioconjugates, a certain period of time is required for the 4-nitrophenolate to adsorb onto the catalyst's surface before the reaction could be initiated. Here we define this period of time as the adsorption time or t_{ads}. After the adsorption time, the reaction becomes stationary and follows first-order rate law. The apparent rate constant (k_{app}) is calculated from the linear slope of the curve and in the following we shall discuss it in terms of L–H model.

The mutual dependence of k_{app} on the catalytic dose as well as concentration of borohydride and 4-NP is shown in Fig. 5d–f where the solid lines refer to the fits of the experimental data with use of Eq. (10) while the best fitting results are obtained with $k = 4.4 \pm 1.0 \times 10^{-4}$ mol/m^2 s, $k_{4\text{-NP}} = 14000 \pm 200$ L/mol, $k_{BH_4} = 22 \pm 2$ L/mol, $m = 0.9 \pm 0.1$, and $n = 0.6 \pm 0.1$. The orders of the kinetic parameters so determined are quite close to those obtained by Wunder et al. (2010). The k_{app} obtained from the linear slope of the kinetic curves is linearly related to the catalyst dose (shown in Fig. 5d), i.e., the surface area available for catalysis, keeping other parameters such as initial 4-NPA concentration and borohydride concentration the same, which could be rationalized by considering the fact that the catalysis usually takes place on the surface of the Au nanoparticles (Murugadoss and Chattopadhyay 2008). The nonlinear relationship of k_{app} versus c_{BH_4}, i.e., concentration

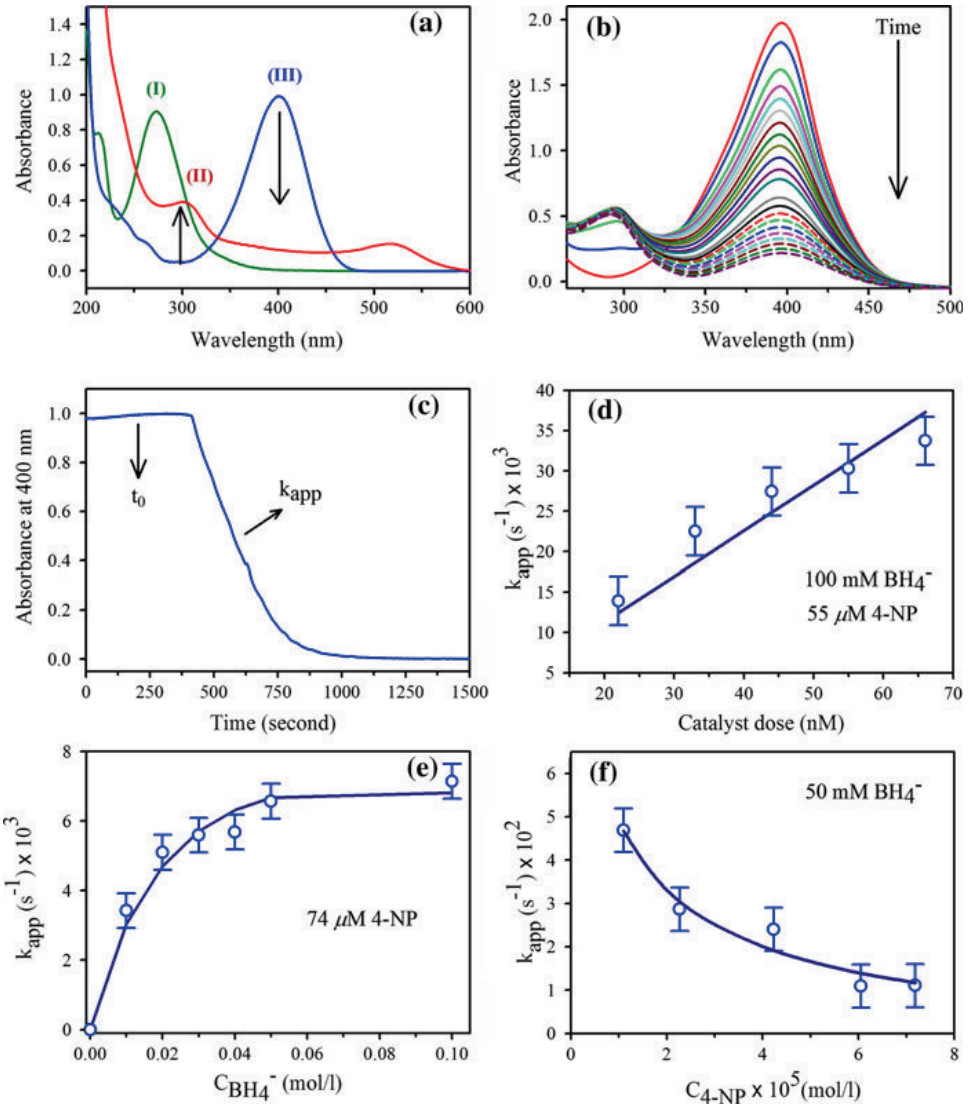

Fig. 5 **a** Absorption spectra of 4-NPA (*I*) in absence of $NaBH_4$, (*II*) in presence of $NaBH_4$ at 0 min, and (*III*) in presence of Au@protein nanobioconjugates. Conditions: $[4\text{-NP}^-] = 5.5 \times 10^{-5}$ M; [Au NPs] $= 2.2 \times 10^{-7}$ M; $[NaBH_4] = 0.1$ M. **b** Concentration versus time plot (monitored at 400 nm) for 4-NPA reduction by $NaBH_4$. Conditions: $[4\text{-NP}] = 5.5 \times 10^{-5}$ M; $[NaBH_4] = 0.1$ M. **c** Typical time dependence of the absorption of 4-NPA at 400 nm. **d** Plot of apparent rate constant (k_{app}) versus catalyst dose for 4-NPA reduction by $NaBH_4$ in the presence of Au@protein solution as catalyst. Conditions: [4-NP] $= 5.5 \times 10^{-5}$ M; $[NaBH_4] = 0.1$ M. **e**, **f** Dependence of the apparent rate constant k_{app} on the concentration of BH_4^{-1} **e** and 4-NP **f**. The *solid lines* are the fit of the Langmuir–Hinshelwood model. The surface area of Au nanoparticles is 0.0106 m^2/L in both cases

of borohydride and the saturation at high concentrations, shown in Fig. 5e, clearly demonstrates the diffusion of the borohydride to the nanoparticles. The effect of 4-NPA concentration on the reduction rate was studied keeping other parameters such as catalyst dose and borohydride concentration unchanged. As depicted in Fig. 5f, in the case of 4-NP reduction using Au NPs as catalyst, it was found that in the very low concentration range of 4-NP, k_{app} decreased with the increase of 4-NP concentration, and in the high concentration range k_{app} remained constant. This is due to high concentration of 4-NP leads to almost full coverage of the surface of the nanoparticles. This slows down the reaction with the borohydride ions on the surface of the Au NPs. Figure 5e and f, clarifies the mutual relationship of k_{app} with c_{BH_4} and $c_{4\text{-NP}}$ which demonstrates that there must be a competition between the reactants on the catalyst's surface.

Moreover, the fitted data in Fig. 5d–f clearly demonstrate that the reduction of 4-NP can be described by the L–H model with good accuracy.

Conclusion

Detail understanding of the associated biochemistry of the proteins during the formation of inorganic nanoparticles has been successfully demonstrated. A number of proteins have been investigated to show the possible effects and it has been found that induction time may increase as the melting temperature of a protein is increased. This suggests that low melting temperatures may be important for the nucleation and growth of nanoparticle. An autocatalytic model has been proposed that fits well with the experimental data and suggest that some nucleations are slowly formed during the induction period that boosts the growth of the nanoparticles. Finally, we have demonstrated that the catalytic reduction of 4-NPA by borohydride in the presence of Au NPs can be modelled in terms of the Langmuir–Hinshelwood model. All the parameters related to this model have been described here in a very efficient way. We hope that with the continuing efforts toward understanding the mechanism of protein–nanoparticle growth relationship is likely to find use in protein biochemistry, thereby making these studies much more widely accessible in nano-biotechnology.

Acknowledgment Nirmal Goswami thanks CSIR, India for fellowship. We thank DST for a financial grant (SR/SO/BB-15/2007).

References

Belohlav Z, Zamostny P (2000) A rate-controlling step in Langmuir–Hinshelwood kinetic models. Can J Chem Eng 78:513–521

Bohren CF, Huffman DR (1983) Absoption and scattering of light by small particles. Wiley, NewYork

Burda C, Chen X, Narayanan R, El-Sayed MA (2005) Chemistry and properties of nanocrystals of different shapes. Chem Rev 105:1025–1102

Dhawan A, Muth JF (2006) Plasmon resonances of gold nanoparticles incorporated inside an optical fibre matrix. Nanotechnology 17:2504–2511

Dinda E, Rashid MH, Mandal TK (2010) Amino acid-based redox active amphiphiles to in situ synthesize gold nanostructures: from sphere to multipod. Cryst Growth Des 10:2421–2433

Doyle WT (1958) Absorption of light by colloids in alkali halide crystals. Phys Rev 111:1067–1072

Drummond PD, Vaughan TG, Drummond AJ (2010) Extinction times in autocatalytic systems. J Phys Chem A 114: 10481–10491

El-Brolossy TA, Abdallah T, Mohamed MB, Abdallah S, Easawi K, Negm S, Talaat H (2008) Shape and size dependence of the surface plasmon resonance of gold nanoparticles studied by photoacoustic technique. Eur Phys J 153:361–364

Esumi K, Isono R, Yoshimura T (2004) Preparation of PAMAM- and PPI-metal (silver, platinum, and palladium) nanocomposites and their catalytic activities for reduction of 4-nitrophenol. Langmuir 20:237–243

Fei L, Perrett S (2009) Effect of nanoparticles on protein folding and fibrillogenesis. Int J Mol Sci 10:646–655

Flenniken ML, Uchida M, Liepold LO, Kang S, Young MJ, Douglas T (2009) A library of protein cage architectures as nanomaterials viruses and nanotechnology. Curr Top Microbio Imunnol 327:71–93

Ghosh SK, Pal T (2007) Interparticle coupling effect on the surface plasmon resonance of gold nanoparticles: from theory to applications. Chem Rev 107:4797–4862

Huang ZY, Mills G, Hajek B (1993) Spontaneous formation of silver particles in basic 2-propanol. J Phys Chem 97:11542–11550

Jin RC (2001) Photoinduced conversion of silver nanospheres to nanoprisms. Science 294:1901–1903

Kamal JKA, Behere DV (2002) Thermal unfolding of soybean peroxidase: appropriate high denaturant concentrations induce cooperativity allowing the correct measurement of thermodynamic parameters. J Biol Chem 277: 40717–40721

Katz E, Willner I (2004) Integrated nanoparticle-biomolecule hybrid systems: Synthesis, properties, and applications. Agnew Chem Int Ed 43:6042–6108

Kim H, Pippel E, Gosele U, Knez M (2009) Titania nanostructures fabricated by atomic layer deposition using spherical protein cages. Langmuir 25:13284–13289

Klem MT, Willits D, Solis DJ, Belcher AM, Young M, Douglas T (2005) Bio-inspired synthesis of protein-encapsulated CoPt nanoparticles. Adv Funct Mater 15:1489–1494

Kramer RM, Li C, Carter DC, Stone MO, Naik RR (2004) Engineered protein cages for nanomaterial synthesis. J Am Chem Soc 126:13282–13286

Link S, El-Sayed MA (2000) Shape and size dependence of radiative, properties of gold nanocrystals. Int Rev Phys Chem 19:409–453

Loweth CJ, Caldwell WB, Peng XG, Alivisatos AP, Schultz PG (1999) DNA-based assembly of gold nanocrystals. Agnew Chem Int Ed 38:1808–1812

Luo J, Maye MM, Han L, Kariuki NN, Jones VW, Lin Y, Engelhard MH, Zhong CJ (2004) Spectroscopic characterizations of molecularly linked gold nanoparticle assemblies upon thermal treatment. Langmuir 20: 4254–4260

Malikova N, Pastoriza-Santos I, Schierhorn M, Kotov NA, Liz-Marzan LM (2002) Layer-by-layer assembled mixed spherical and planar gold nanoparticles: control of interparticle interactions. Langmuir 18:3694–3697

Mie G (1908) Contributions to the optics of turbid media, particularly of colloidal metal solutions. Ann Phys 25: 377–445

Mei Y, Sharma G, Lu Y, Ballauff M (2005) High catalytic activity of platinum nanoparticles immobilized on spherical polyelectrolyte brushes. Langmuir 21:12229–12234

Mei Y, Lu Y, Polzer F, Ballauff M (2007) Catalytic activity of palladium nanoparticles encapsulated in spherical polyelectrolyte brushes and core-shell microgels. Chem Mater 19:1062–1069

Mirkin CA, Letsinger RL, Mucic RC, Storhoff JJ (1996) A DNA-based method for rationally assembling nanoparticles into macroscopic materials. Nature 382:607–609

Murugadoss A, Chattopadhyay A (2008) Surface area controlled differential catalytic activities of one-dimensional chain-like arrays of gold nanoparticles. J Phys Chem C 112:11265–11271

Narayanan R, El-Sayed MA (2004) Changing catalytic activity during colloidal platinum nanocatalysis due to shape changes: electron-transfer reaction. J Am Chem Soc 126:7194–7195

Panigrahi S, Basu S, Praharaj S, Pande S, Jana S, Pal A, Gosh SK, Pal T (2007) Synthesis and size-selective catalysis by supported gold nanoparticles: study on heterogeneous and homogeneous catalytic process. J Phys Chem C 111: 4596–4605

Praharaj S, Nath S, Ghosh SK, Kundu S, Pal T (2004) Immobilization and recovery of Au nanoparticles from anion exchange resin: resin-bound nanoparticle matrix as a catalyst for the reduction of 4-nitrophenol. Langmuir 20:9889–9892

Riboh JC, Haes AJ, McFarland AD, Ranjit C, Van Duyne RP (2003) A nanoscale optical biosensor: real-time immunoassay in physiological buffer enabled by improved nanoparticle adhesion. J Phys Chem B 107:1772–1780

Saha S, Pal A, Kundu S, Basu S, Pal T (2010) Photochemical green synthesis of calcium-alginate-stabilized Ag and Au nanoparticles and their catalytic application to 4-nitrophenol reduction. Langmuir 26:2885–2893

Shafer-Peltier KE, Haynes CL, Glucksberg MR, Van Duyne RP (2003) Toward a glucose biosensor based on surface-enhanced raman scattering. J Am Chem Soc 125:588–593

Shang L, Wang Y, Jiang J, Dong S (2007) pH-Dependent protein conformational changes in albumin: gold nanoparticle bioconjugates: a spectroscopic study. Langmuir 23:2714–2721

Storhoff JJ, Elghanian R, Mucic RC, Mirkin CA, Letsinger RL (1998) One-pot colorimetric differentiation of polynucleotides with single base imperfections using gold nanoparticle probes. J Am Chem Soc 120:1959–1964

Sun Y, Xia Y (2002) Shape-controlled synthesis of gold and silver nanoparticles. Science 298:2176–2179

Tan YN, Lee JY, Wang DIC (2010) Uncovering the design rules for peptide synthesis of metal nanoparticles. J Am Chem Soc 132:5677–5686

Tian N, Zhou ZY, Sun S-G, Ding Y, Wang ZL (2007) Synthesis of tetrahexahedral platinum nanocrystals with high-index facets and high electro-oxidation activity. Science 316:732–735

Umpleby RJ, Baxter SC, Chen Y, Shah RN, Shimizu KD (2001) Characterization of molecularly imprinted polymers with the langmuir freundlich isotherm. Anal Chem 73:4584–4591

Ung T, Liz-Marzan L, Mulvaney P (2001) Optical properties of thin films of $Au@SiO_2$ particles. J Phys Chem B 105:3441–3452

Vajda S, Pellin JM, Greeley PJ, Marshall LC, Curtiss AL, Ballentine AG, Elam WJ, Catillon-Mucherie S, Redfern CP, Mehmood F, Zapol P (2009) Subnanometre platinum clusters as highly active and selective catalysts for the oxidative dehydrogenation of propane. Nat Mater 8: 213–216

Wunder S, Polzer F, Lu Y, Mei Y, Ballauff M (2010) Kinetic analysis of catalytic reduction of 4-nitrophenol by metallic nanoparticles immobilized in spherical polyelectrolyte brushes. J Phys Chem C 114:8814–8820

Xie JP, Zheng YG, Ying JY (2009) Protein-directed synthesis of highly fluorescent gold nanoclusters. J Am Chem Soc 131:888–889

Xu W, Kong JS, Yeh Y-TE, Chen P (2008) Single-molecule nanocatalysis reveals heterogeneous reaction pathways and catalytic dynamics. Nat Mater 7:992–996

Xu W, Kong JS, Chen P (2009) Single-molecule kinetic theory of heterogeneous and enzyme catalysis. J Phys Chem C 113:2393–2404

Zeman EJ, Schatz GC (1987) An accurate electromagnetic theory study of surface enhancement factors for silver, gold, copper, lithium, sodium, aluminum, gallium, indium, zinc, and cadmium. J Phys Chem 91:634–643

Zhang H, Li X, Chen G (2009) Ionic liquid-facilitated synthesis and catalytic activity of highly dispersed Ag nanoclusters supported on TiO_2. J Mater Chem 19:8223–8231